Synthesis and Microphase Separation of PS-*b*-P(MA-*alt*-St) Block Copolymers and Their Ionomers for the Design of Polymer Crystallization Nucleation Agents

Shili Xing, Rui Li, Ping Tang*

Several well-controlled polystyrene-*block*-poly(styrene-*alt*-maleic anhydride) (PS-*b*-P(St-*alt*-MA)) functionalized block copolymers (BCs) and their sodium salt ionomers with different block ratios and molecular weights are synthesized through two-step reversible addition–fragmentation chain transfer (RAFT) polymerization. The atomic force microscopy (AFM) images and differential scanning calorimetry (DSC) results reveal that the prepared BCs and their ionomers microphase separate into various nanostructures depending on the block ratios. By taking advantage of the formation of amphiphilic nanostructures via the microphase, the block ionomers serve as nucleation agents to improve the crystallization rate of poly(ethylene terephthalate) (PET). The crystallization behavior of PET upon the addition of block ionomers is investigated isothermally and non-isothermally by DSC. The results show that the block ionomers can effectively accelerate the crystallization rate of PET, which strongly depends on the molecular weights and block ratios

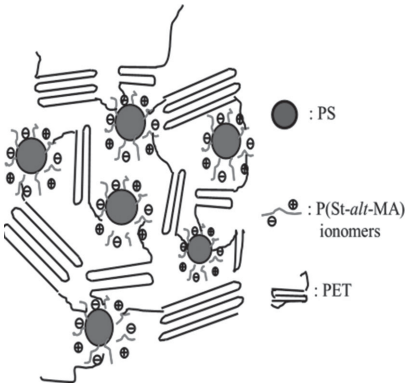

1. Introduction

Due to advances in controlled free radical polymerization in recent decades, block copolymers (BCs) have found numerous applications ranging from thermoplastic elastomers, adhesives, surfactants, compatibilizers in polymer blends, templating materials, and drug delivery.[1] There is no macroscopic phase separation in BCs. Rather these systems experience microphase separation due to the connectivity of the unlike blocks. These microphase-separated structures are governed by a delicate balance of the interaction energy and the chain stretching and mainly depend on the molecular weight fraction of the constituent blocks and segregation strength denoted by χN, where χ is the Flory–Huggins interaction parameter and N is the polymerization index.[2–5] For BCs in bulk, self-assembled, periodic structures such as body-centered-cubic-packed (bcc) spheres, hexagonal-close-packed (hcp) cylinders, lamellae, and more complex phases have been theoretically predicted and experimentally observed.[5–7]

An important application of BCs is as a compatibilizer for immiscible homopolymers. This makes the systems compatible by taking advantage of the amphiphilic characteristics to interact with both phases. For instance, functionalized BCs consisting of polar maleic anhydride (MA) units often serve as commercial compatibilizers in most immiscible polymer blends. The MA-grafted poly(styrene-*b*-(ethylene-*co*-butylene)-*b*-styrene) block copolymer (SEBS-MA) improves the dispersion of nanomagnesium hydroxide (nano-MH) in isotactic polypropylene (PP)

Dr. S. Xing, Dr. R. Li, Prof. P. Tang
State Key Laboratory of Molecular Engineering of Polymers, Department of Macromolecular Science, Fudan University, Shanghai 200433, China
E-mail: pingtang@fudan.edu.cn

DOI: 10.1002/macp.201400444

by increasing interfacial adhesion between PP and MH nanocomposites.[8]

Ionomers also play an important role as compatibilizers for polymer blending. The compatibility of nylon6 and ethylene vinyl acetate (EVA) blends upon the addition of ionomers known as commercial Surlyn 1601 is significantly improved versus PA6/EVA blends.[9] The interfacial interaction of poly(ethylene-*co*-vinyl alcohol) (EVOH) and poly(ethylene-*co*-methacrylic acid) with 15% acid content neutralized with zinc salt is effectively enhanced.[10] Therefore, functionalized BCs that can be easily made into ionomers attract more interest in enhancing interfacial interactions between two immiscible polymer components.

BCs containing MA have the excellent properties with applications in synthesis,[11] physical characteristics,[12–14] etc. Benoit et al.[11] reported polystyrene-*block*-poly(styrene-*ran*-maleic anhydride) copolymers that were synthesized by a living free radical method.[13] Polystyrene-*block*-poly(styrene-*alt*-maleic anhydride) (PS-*b*-P(St-*alt*-MA)) copolymers with highly alternating styrene and MA sequences were synthesized by a one-step method via nitroxide-mediated polymerization.[11] Bapat and co-workers[15,16] synthesized PS-*b*-P(St-*alt*-MA) copolymers via the one-pot reversible addition–fragmentation chain transfer (RAFT) polymerization using dodecylsulfanylthiocarbonyl sulfanyl-2-methylpropionic acid (DMP) as chain transfer agent. The prepared PS-*b*-P(St-*alt*-MA) copolymers can reversibly assemble into stars and miktoarm stars nanostructures by dynamic-covalent disulfide linkages capable of redox-induced cleavage/reassembly. Han et al.[12] synthesized PS-*b*-P(St-*alt*-MA) copolymers by RAFT polymerization using the dithioester chain transfer agent (S)-benzyl dithiobenzoate (BTBA). The hydrolyzed amphiphilic BC formed novel micelle-like nanoparticles through self-assembly in aqueous media. Unfortunately, the microphase separation of PS-*b*-P(St-*alt*-MA) copolymers and their applications such as nucleation agents have not been reported.

Using the above results as a foundation, we suggest that the excellent properties of PS-*b*-P(St-*alt*-MA) copolymers including functionalization, microphase separation, and self-assembly will allow them to act as polymer nucleation agents. It is known that poly(ethylene terephthalate) (PET) is a low-cost linear semicrystalline thermoplastic polyester with excellent mechanical, physical, and chemical properties.[17] However, the crystallization rate of PET is rather slow, and the crystallization temperature is high resulting in a high mold temperature for injection molding processing. This limits its commercial utility especially in engineering plastic applications. The addition of nucleation agents and nucleation-promoting agents is one of the most efficient means to improve the crystallization rate.

Many papers in this field focus on providing more nucleation sites to improve the crystallization rate.[18–21] Most of the nucleation agents for PET are low- molecular-weight organics,[22] inorganic compounds,[23] and ionomers.[24,25] Of these, ionomers are the most widely used and improve the crystallization behavior of PET because they have excellent compatibility with PET and provide many nucleation sites for polymer crystallization. Ethylene-sodium methacrylate (trade name Surlyn resin) is the most widely used ionomer in PET injection molding.[25] For amphiphilic diblock copolymers, the aggregation of the hydrophobic chain in aqueous media promotes the dispersion of hydrophilic chains around the aggregation core assembled by hydrophobic chains. Lin et al. reported the unimolecular star-like nanostruces composed of inner coil-like blocks and outer rod-like blocks crafted by combination of living polymerization with click chemistry.[26,27] Moreover, the incorporation of diblock copolymer into a semicrystallizable polymer system — termed crystalline-amorphous (C-A) copolymer — exhibits microphase separation through interactions between one block chain and one bulk polymer.[2,28–32] In addition, the incorporation of BC into the semicrystallizable homopolymers results in extra aggregation of the A blocks to achieve micelles driven by microphase separation. This can serve as nucleation sites or colloidal nanocrystals for C component crystallization.[2,33,34] The immiscible block of the block ionomers can assemble into the microdomain due to incompatibility with the polymer matrix, while the miscible blocks disperse into the matrix. This microphase-separated structure can act as nucleus initiating the crystal growth. In contrast to previous applications as a compatibilizer and thermoplastic elastomer, in this paper, PS-*b*-P(St-*alt*-MA) diblock ionomers are designed as the nucleation agent to induce crystallization of PET according to the crystallization theory and our previous research.[35] The nucleation interface energy is reduced due to the good miscibility between MA unit and PET.

The molecular weight, block composition, and chain architecture strongly determine the self-assembled nanostructures of BCs,[36] which influence nucleation efficiency when added as nucleation agents. Therefore, PS-*b*-P(St-*alt*-MA) BCs with a series of molecular weights and block ratios were synthesized by RAFT polymerization, and their ionomers were prepared by acid–base reactions. The structures and microphase separation of BCs and their ionomers were investigated with differential scanning calorimetry (DSC) and atomic force microscopy (AFM). We investigated the nucleation efficiency of various block ionomers as nucleation agent for PET via isothermal and nonisothermal crystallization.

2. Experimental Section

2.1. Materials

MA and α,α′-azobis(isobutyronitrile) (AIBN) were purchased from Alfa Aesar and were recrystallized at least three times in chloroform and methanol, respectively. Styrene (St) and cyclohexanone were obtained from the Sinopharm Chemical Reagent Co., Ltd and redistilled under reduced pressure to remove water and inhibitor. Carbon disulfide (CS_2) from Shanghai 4th Factory of Chemicals (99%) was purified by vigorously shaking with $KMnO_4$ (0.4 wt% based on CS_2) followed by filtration and distillation to collect a colorless fraction. Tetrahydrofuran (THF) from Shanghai Qiangsheng Chemicals (99%) was dried by sodium with further vacuum distillation before use. The α-methylstyrene (99%) and bromobenzene (99%) were purchased from Acros. Petroleum ether (60 °C –90 °C) and ammonia water (25 wt%) were purchased from Sinopharm Chemical Reagent Co., Ltd. Other chemicals were purchased from the Sinopharm Chemical Reagent Co., Ltd. and all of them were analytical reagents and used without any treatment. PET with intrinsic viscosity of 0.9 dL g^{-1} was produced by Sinopec Yizheng Chemical Fiber Company Limited, China.

2.2. Synthesis of PS-*b*-P(St-*alt*-MA) via RAFT Polymerization

The BCs were prepared by the two-step RAFT polymerization at 60 °C with the cumyl dithiobenzoate (CDB) as a dithioester chain transfer agent and AIBN as an initiator. The synthesis of CDB was from literature.[37] The synthesis of the copolymers is shown in Scheme 1.

First, the PS-RAFTs were synthesized to obtain the dithioester-capped (living end) polystyrene. The feeding mole ratios of St to CDB to AIBN are 200/2/1–2000/2/1. The reaction mixtures were deoxygenated by three cycles of freeze–pump–thaw, backfilled with nitrogen, and then heated to 60 °C. Aliquots were collected at various time points for gel permeation chromatography (GPC) analysis. The reaction was quenched in liquid nitrogen to stop the polymerization when the molecular weight of the PS-RAFTs reached the desired molecular weight. The reaction product was then added dropwise into methanol, precipitated, and concentrated. The PS-RAFTs were redissolved in THF and added to methanol, for a replicate precipitation/concentration step. This process was repeated at least three cycles to purify the PS-RAFTs.

Second, the PS-*b*-P(St-*alt*-MA) copolymers were synthesized based on the PS-RAFTs with St/MA/PS-RAFT/AIBN monomer molar feeding ratio of 200/200/2/1–1000/1000/2/1. In this process, the MA does not actually homopolymerize[38] because

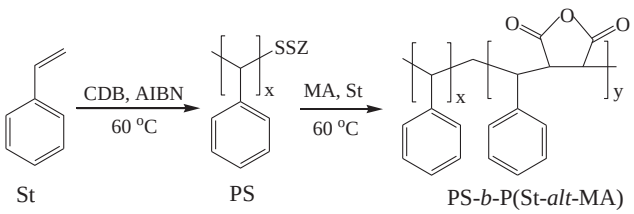

Scheme 1. Synthesis of block copolymers with RAFT polymerization.

reactivity ratio between St and MA is $r_1 = 0.121 \pm 0.003$ (ratio of St homopolymerization rate to St/MA copolymerization). The $r_2 = 0.009 \pm 0.001$ for free radical polymerization (ratio of MA homopolymerization rate to St/MA copolymerization).[39] Therefore, MA copolymerization with St alternates especially at the feeding mole ratio of St:MA of 1:1 used here. BCs with various chain lengths have been obtained by changing the polymerization time and molar feed ratios. The molecular weights of PS-*b*-P(St-*alt*-MA) copolymers via GPC are similar to the last process. The purification process is also the same as used for PS-RAFTs. The final collected copolymer powders were dried under vacuum at 60 °C for at least 24 h.

2.3. Preparation of PS-*b*-P(St-*alt*-MA) Block Ionomers and PET/Ionomers Blends

First, a methanolic solution of sodium hydroxide was added dropwise to a copolymer solution of dioxane (0.1 g mL^{-1}) at room temperature until the solution pH reached alkalescence to ensure the anhydride was completely changed to a carboxylate. Second, the prepared PS-*b*-P(St-*alt*-MA) ionomers (BIs) solution was added dropwise to petroleum ether, and the ionomers were precipitated from solution. The final products were dried at 60 °C in a vacuum oven for 24 h. The PET pellets were dried at 110 °C for 24 h in a vacuum oven prior to use, and then mixed with 1 wt% block ionomers in an internal batch mixer of the Kechuang XSS-300 torque rheometer at 280 °C with a twin-screw speed of 80 rpm for 5 min. Next, the composites were removed and quickly quenched in iced water for further studies.

2.4. General Characterization and Measurements

The molecular weight (M_w) and polydispersity index (PDI) of the prepared BCs were determined by GPC with THF as the solvent at a flow rate of 1.0 mL min^{-1} at room temperature on an HP 1100 with a series of columns (Phenogel 100A, Phenogel 100 KA, and Phenogel mix) equipped with refractive index (RI) and ultraviolet (UV) detectors. The injection volume was 20 μL of 5‰ copolymers in THF. The M_w and PDI were based on a linear calibration curve constructed with polystyrene standards with low polydispersity (M_n = 800, 2000, 4000, 9000, 30 000, 50 000, 100 900, and 233 000). Fourier transform-infrared (FTIR) spectra were recorded on a Nicolet 6700 with DTGS detector between 400 and 4000 cm^{-1} with 64 replicates taken at 4 cm^{-1} resolution.

The ^1H NMR and ^{13}C NMR spectra were recorded on a Bruker DMX 500 MHz at 25 °C with acetone-d_6 as the solvent and a resonance frequency of 500 MHz to study the block ratio of PS to P(St-*alt*-MA) and sequence distribution. For analysis of sequence distribution, overlapping peaks were integrated after Lorentzian deconvolution of the spectra using the deconvolution option implemented in the MestReNova NMR software. The thermal stability behavior of the PS-*b*-P(St-*alt*-MA) ionomers was investigated with a TA thermogravimetric analyzer (TGA) Q5000 instrument at a heating rate of 20 °C min^{-1} from room temperature to 700 °C under nitrogen. The glass transition temperatures (T_gs) of BCs and ionomers were determined by thermal analysis with a TA instrument DSC-Q2000 in nitrogen atmosphere. Samples were heated to at least 30 °C above their

component T_g values and held at that temperature for 5 min to erase the previous thermal history. Samples were then cooled to 0 °C at rate 20 °C min^{-1} and held at that temperature for 5 min and then reheated at a rate of 10 °C min^{-1} (second heat) to at least 30 °C above their component T_g values. The T_gs of samples were extracted from second heat scan.

The morphology of the BC film nanostructures was investigated by AFM (Nanoscope VIII) operating in tapping mode. The diblock copolymers were dissolved in cyclohexanone at 1 wt%. The polymer films were prepared by spin-coating the solution onto silicon wafers cleaned with a 70/30 (v/v) solution of 98% H_2SO_4/30% H_2O_2 at 80 °C for 1 h and then thoroughly rinsed with deionized water and dried prior to spin-coating. Before thermal annealing, the prepared film surfaces were observed by AFM. The height differences in the film surfaces are below 2 nm implying very flat surfaces (not shown here). The prepared film is then used to study the microphase separation by AFM under thermal annealing.

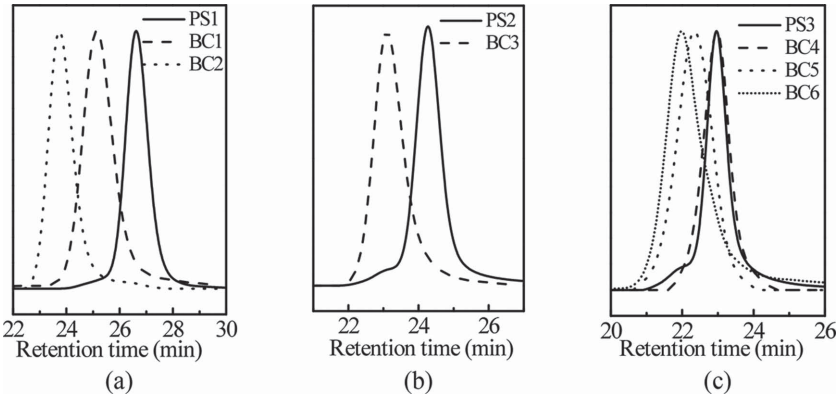

Figure 1. GPC profiles of block copolymers extended from the PS-RAFT agents. The solid lines represent PS-RAFT in the first step and the dotted lines for PS-*b*-P(St-*alt*-MA) block copolymers after the second-stage polymerization.

2.5. DSC Study of Crystallization Behavior

The isothermal and nonisothermal crystallization behaviors of PET-based samples were investigated with a TA instrument DSC-Q2000 under nitrogen. To investigate the isothermal melt-crystallization and melting behavior, samples (3–5 mg) were heated to 280 °C rapidly and maintained for 5 min to erase the previous thermal history under the standard mode for DSC and then cooled to the selected crystallization temperature (T_c) at 200 °C min^{-1} and maintained at that temperature for at least 60 min for complete crystallization. The enthalpy evolved during the isothermal crystallization was recorded as a function of time at different T_c values. To investigate the nonisothermal crystallization, the samples had to erase their previous thermal history and then cooled at various rates from 280 °C to 50 °C to observe nonisothermal melt-crystallization behavior (cooling curve). The DSC data were analyzed by TA universal analysis software.

3. Results and Discussion

3.1. Molecular weights and PDIs of PS-*b*-P(St-*alt*-MA) Copolymers

We synthesized a series of PS-*b*-P(St-*alt*-MA) BCs with different molecular weights and compositions by the two-step RAFT polymerization with CDB as the dithioester chain transfer agent (Scheme 1). We used these products to systemically study the effect of molecular weights and polymer compositions on microphase separation of BCs. We prepared six copolymers with various average molecular weights and narrow polydispersities by changing the monomer-to-initiator ratio and controlling the reaction time.

Figure 1 shows the GPC curves of the PS-RAFTs synthesized in the first step and the final PS-*b*-P(St-*alt*-MA) BCs from the PS-RAFT agents after the second step. The corresponding values are listed in Table 1. BCs denoted as BC1 and BC2 are extended from the PS-RAFT agent with a molecular weight of 3590 g mol^{-1}; BC3 is extended from the PS-RAFT agent with a molecular weight of 10 970 g mol^{-1}; BC4, BC5, and BC6 are extended from the PS-RAFT agent with a molecular weight 21 810 g mol^{-1}. Figure 1 illustrates that the GPC curves of PS-*b*-P(St-*alt*-MA) BCs shift left versus the first-step PS-RAFTs due to higher molecular weight. Moreover, all the final BCs show sharp single peaks indicating that the copolymers have negligible PS homopolymer contamination. Furthermore, all the PDIs (M_w/M_n) of the final BCs are very narrow from 1.02 to 1.25 shown in Table 1 indicating that the copolymerization of St and MA with CDB as the dithioester chain transfer agent produces controlled radical polymerization. Therefore, our two-step RAFT polymerization can obtain well-defined PS-*b*-P(St-*alt*-MA) BCs with different molecular weights and block ratios to act as nucleation agent for PET. The molecular weight ratios of the PS block to P(St-*alt*-MA) block can be calculated based on the GPC results and further verified through ^{1}H NMR in Table 1.

3.2. Structure of the PS-*b*-P(St-*alt*-MA) Block Copolymers

From the FTIR spectra of the BCs shown in Figure 2a, the strong absorption peaks at 1778 and 1857 cm^{-1} are characteristic of the anhydride.[40,41] The peaks at 1455, 1495, and 1600 cm^{-1} correspond to the phenyl ring. The peaks at 2920 and 3030 cm^{-1} are assigned to the absorption of methine and methylene on the polymer chain.[42,43] This suggests that the BCs have been synthesized successfully. The FTIR spectra of corresponding block ionomers in Figure 2b show

Table 1. Molecular characteristics of PS-*b*-P(St-*alt*-MA) block copolymers.

Block copolymer	M_W^{1} [a)] [g mol^{-1}]	PDI^{1} [b)]	M_W^{2} [a)] [g mol^{-1}]	PDI^{2} [b)]	M_W ratio [c)]	M_W ratio [d)]
BC1	3590	1.08	7010	1.07	1.05	1.19
BC2	3590	1.07	14 420	1.07	0.33	0.37
BC3	10 970	1.08	20 010	1.06	1.21	1.23
BC4	21 810	1.04	24 250	1.09	8.95	9.26
BC5	21 810	1.12	31 610	1.09	2.23	2.31
BC6	21 810	1.24	39 300	1.09	1.24	1.29

[a)] M_W^1: Weight-average molecular weight of PS-RAFT after the first step; M_W^2: Weight-average molecular weight of PS-*b*-P(St-*alt*-MA) after the second step; [b)]PDI^1: Polydispersity index of PS-RAFT after the first step; PDI^2: Polydispersity index of PS-*b*-P(St-*alt*-MA) after the second step; M_W ratio; [c)]Molecular weight ratio of the first block PS and second block P(St-*alt*-MA) calculated by GPC; M_W ratio; [d)]Molecular weight ratio of the first block PS and second block P(St-*alt*-MA) by ^{1}H NMR based on Equation 1 and 2.

a strong absorption at 3432 cm^{-1} due to absorption of carboxylate. Moreover, peaks corresponding to the structure of the BCs are slightly blue-shifted due to salinization.

The compositions of the BCs were determined with ^{1}H NMR (Figure 3a) with the chemical shift of the copolymer protons marked in the spectra. The chemical shift of the phenyl proton is about 7.0 ppm. The proton of MA is about 3.3 ppm, and the other protons of the —CH— and —CH_2— groups on the backbone chains are within 1.2–2.8 ppm. The molecular weight ratio of the two blocks can be calculated based on the integrated area under the corresponding peaks of proton H_c and H_d, respectively. We assumed that the mole ratio of the PS block to the P(St-*alt*-MA) block was *x*:1, which can be calculated in Equation 1. Second, the molecular weight ratio of the two blocks can be calculated according to Equation 2 because the final object BC is an alternating polymer as explained above. The relative molecular weights of MA and St are 98 and 104 g mol^{-1}, respectively.

$$\frac{2}{5+5x} = \frac{\text{Integrated area}_{(H_c)}}{\text{Integrated area}_{(H_d)}} \quad (1)$$

$$\frac{M_{w(PS)}}{M_{W[P(St\text{-}alt\text{-}MA)]}} = \frac{104x}{202} \quad (2)$$

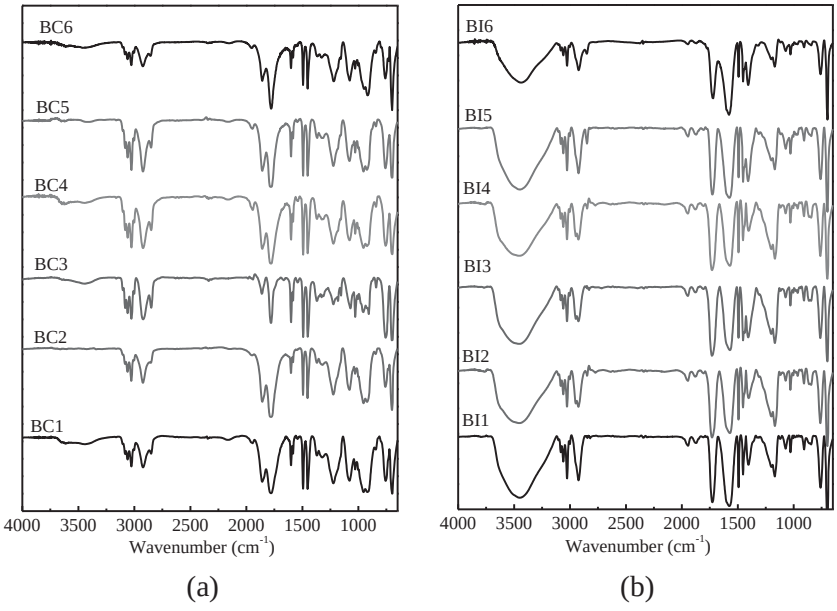

Figure 2. FTIR spectra: a) block copolymers; b) block ionomers.

The calculated molecular weight ratios between the two blocks according Equation 1 and 2 are nearly consistent with the GPC results shown in Table 1. In order to synthesize a series of PS-*b*-P(St-*alt*-MA) BCs with different molecular weights and compositions, different feed ratios of monomers as well as reaction times were designed in this process. The feed ratios of the St to CDB to AIBN for PS1, PS2, and PS3 are 200:2:1, 1000:2:1, and 2000:2:1, respectively. The conversion ratio of St is less than 40% to obtain PS-RAFT systems with small PDI values. The conversion ratios for PS1, PS2, and PS3 are about 36%, 22%, and 22%, respectively. Obviously, the molecular weight of PS-RAFT is increasing with increasing St to CDB feed ratio. For the second step, the St:MA:PS-RAFT:AIBN monomer mole feed ratio for BC1 is 200:200:2:1, and the

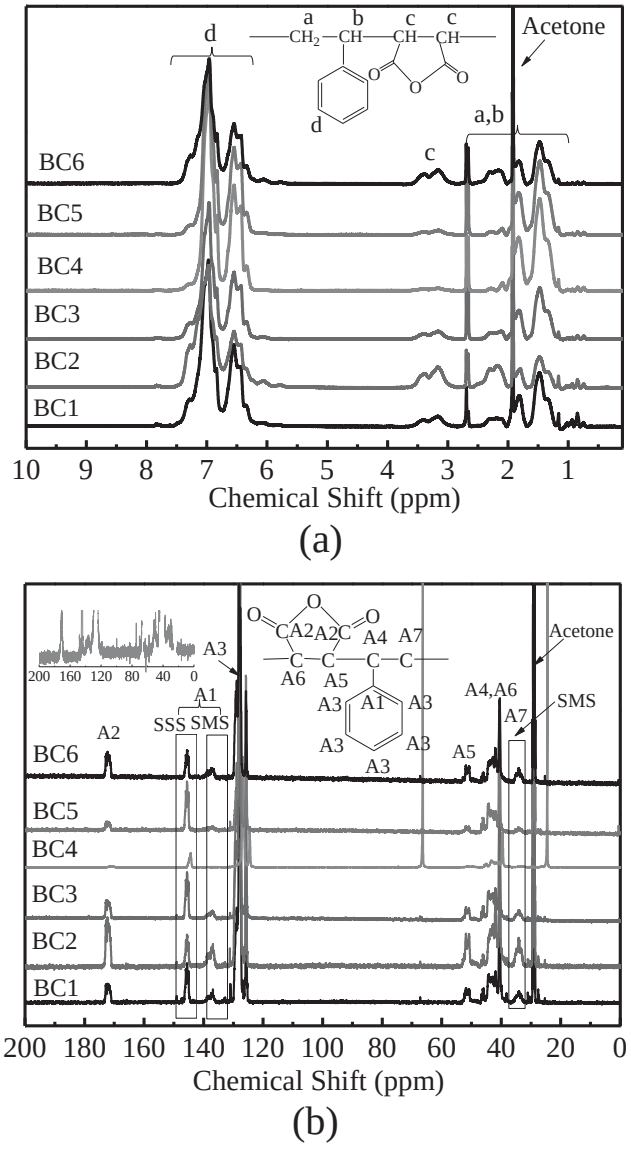

Figure 3. NMR spectra of block copolymers with peak assignments: a) ^{1}H NMR; b) ^{13}C NMR.

conversion ratio is about 17%. The monomer feed ratios of BC2, BC3, BC4, and BC5 are 400:400:2:1 and the conversion ratios are about 27%, 23%, 6%, and 25%, respectively. The molecular weight increases with the increase in conversion ratio under the same feed ratios. The monomer feed ratio of BC6 is 1000:1000:2:1, and the conversion ratio is about 17%. Therefore, diblock copolymers with tunable compositions can be obtained by controlling the molar feed ratio and reaction time through well-controlled RAFT polymerization.

Figure 3b shows ^{13}C NMR spectra of PS-*b*-P(St-*alt*-MA) BCs with structural assignments from literature.[11,44] We choose THF-d_8 as the solvent to characterize the ^{13}C NMR for BC4 (high molecular weight of polystyrene block and low molecular weight of P(St-*alt*-MA) block) due to its poor solubility in acetone-d_6. The others were dissolved in acetone-d_6 for ^{13}C NMR. The triad sequences of BCs were determined via the chemical shifts of characteristic carbons in MA and St, as shown in Figure 3b.

There are two predominant peaks. The first is the resonance representing the aromatic carbon closest to the backbone belonging to the St, which is labeled A1 in Figure 3b. The second is the resonance of the —CH_2— group on the aliphatic backbone belonging to St-labeled A7 in Figure 3b. The perfectly alternating sequence (SMS) shows an obvious A1 resonance at 137–140 ppm and an obvious A7 resonance at 33–37 ppm. The SSS sequence shows an obvious A1 resonance at 145–148 ppm. From Figure 3b, the ^{13}C NMR spectra reveal two significant populations of triads corresponding to the SMS alternating sequences and SSS homopolystyrene sequences. This confirms that our copolymers are PS-*b*-P(St-*alt*-MA).

3.3. Microphase Separation of PS-*b*-P(St-*alt*-MA) Block Copolymers and Their Ionomers

We design the nucleating agents for PET by taking advantage of the microphase- separated nanostructure. The nucleating effects are related with the microphase-separated structures, which strongly depends on the molecular weight and copolymer composition. Therefore, we synthesized PS-*b*-P(St-*alt*-MA) BCs with a series of molecular weights and block ratios. Obviously, PS blocks will separate from PET, while P(St-*alt*-MA) block mix with PET, thus forming core–shell structure in PET matrix, which can serve as the nucleation sites for PET to crystallization. Crystal nuclei are typically small and transient and they are difficult to be detected in experiments.[45] Furthermore, the microphase-separated structures of PS-*b*-P(St-*alt*-MA) block ionomers in PET matrix used to provide nucleation sites are not easy to be obtained in experiments. Therefore, we studied the microphase separation of PS-*b*-P(St-*alt*-MA) BCs and ionomers in the bulk, which is a prerequisite for microphase separation in the polymer matrix.

Block copolymers with chemically different block species can microphase separate and self-assemble into a wide variety of nanostructures. To investigate the microphase-separated two-phase structures, the T_gs of BCs were investigated with DSC. The DSC heat flow curves for all BCs and their ionomers are shown in Figure 4a,b, respectively. The T_gs of the two blocks are generally close to that their corresponding homopolymers. This is unlike the random copolymers that show a single T_g.[46]

From the DSC curves in Figure 4a, BC3, BC4, BC5, and BC6 display two distinct responses—one near $T_g \approx 110$ °C corresponding to PS[47,48] and the other $T_g \approx 156$ °C corresponding to P(St-*alt*-MA).[49] The T_g of P(St-*alt*-MA) is higher than PS due to the strong intermolecular forces generated from the polarity of the MA. For BC1 and BC2,

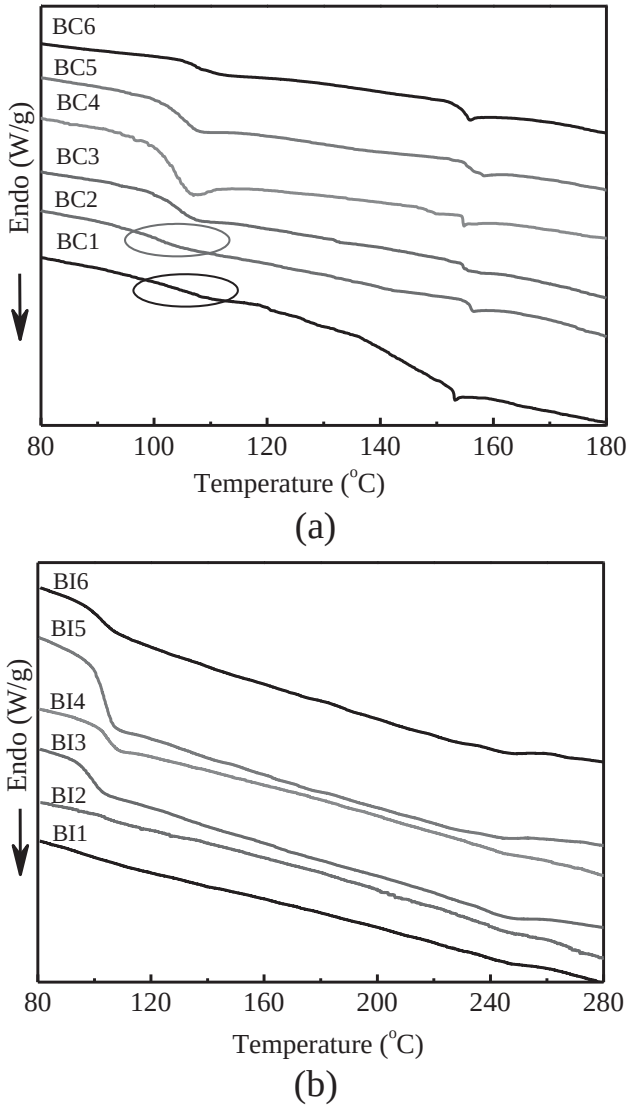

Figure 4. DSC curves of the second scan at a heating rate of 10 °C min^{-1} for a) PS-*b*-P(St-*alt*-MA) block copolymers and b) block ionomers.

the T_g of the PS block is not obviously due to its short-chain length, but only with an obvious response corresponding to the P(St-*alt*-MA). Furthermore, the two transitions corresponding to each BC are different reflecting the relative comonomer compositions. The results suggest that BC3, BC4, BC5, and BC6 exhibit obvious microphase separation, but no obvious phase separation for BC1 and BC2 are seen due to their low molecular weight of PS blocks. Although the molecular weight of P(St-*alt*-MA) blocks in BC4 is also very low, the strong intermolecular force promotes microphase separation and thus shows two T_g transitions. Versus the corresponding BCs, the block ionomers also exhibit two T_g values. However, the T_g of the PS block is nearly unchanged. Salinization increase the polarity of the alternating BCs, which improves the T_g of P(St-*alt*-MA) block from 156 °C to 241 °C as shown in Figure 4b. Therefore, the P(St-*alt*-MA) block ionomers remain solid state when acting as a nucleation agent for PET during crystallization.

To further investigate the microphase-separated morphologies of PS-*b*-P(St-*alt*-MA) copolymers and ionomers, we performed tapping mode AFM experiments on the sample films. Several different annealing temperatures (from 160 °C to 200 °C) were chosen in this process, which were slightly higher than the T_g of both blocks determined by DSC. The phase images of BCs annealed at 180 °C and 200 °C are not shown here due to quite fuzzy phase-separated interfaces. The phase images of BCs annealed at 170 °C are shown in Figure S1 (Supporting Information). Figure 5 shows the phase images of these BCs after thermal annealing at 160 °C for 2 d. From the AFM height images of these BCs after thermal annealing at 160 °C (Figure S2, Supporting Information), the height range is 2–6 nm, which indicates that the surfaces of the annealed thin films are fairly flat and the nanostructures of the phase image are due to microphase separation of the BCs. Combining Figure 5 and Figure S1 (Supporting Information), BCs microphase separate to form various nanostructures dependent on the block composition after thermal annealing. The phase images from samples annealed at 160 °C are clearer with a sharp interface due to the larger interaction parameter χ (inverse relation with temperature) in contrast to annealing at 170 °C. Samples BC1 in Figure 5a, BC3 in Figure 5c, and BC6 in Figure 5f are all striated. The nanostructure sizes are approximately 10, 17, and 23 nm, respectively. This increases with increasing molecular weight; BC2 in Figure 5b, BC4 in Figure 5d, and BC5 in Figure 5e form droplet-like morphologies. Therefore, PS-*b*-P(St-*alt*-MA) BCs can form microphase separation morphologies dependent on the molecular weight fraction of the PS block.

In contrast to PS-*b*-P(St-*alt*-MA) BCs, the interaction parameter χ between the two blocks of PS-*b*-P(St-*alt*-MA) block ionomers is higher than PS-*b*-P(St-*alt*-MA) BCs, which make the block ionomers form smaller microdomains.[50] However, the study of block ionomers under heat annealing is difficult because the blocks have disparate polarities and it is difficult to choose cosolvents for these two blocks resulting in thin films on silicon. We solved this dilemma by using solvent annealing to switch the polarity after spin coating PS-*b*-P(St-*alt*-MA) BC film via a subsequent chemical reaction.

For example, a carboxylic acid amine salt was used to replace the carboxylic acid sodium salt and study the microphase separation of block ionomers. We first prepared PS-*b*-P(St-*alt*-MA) BC thin films and then placed them in a glass vessel with a condenser tube. The vessel was quickly closed after adding 50 mL of ammonia and the thin film should be placed at the top of ammonia.

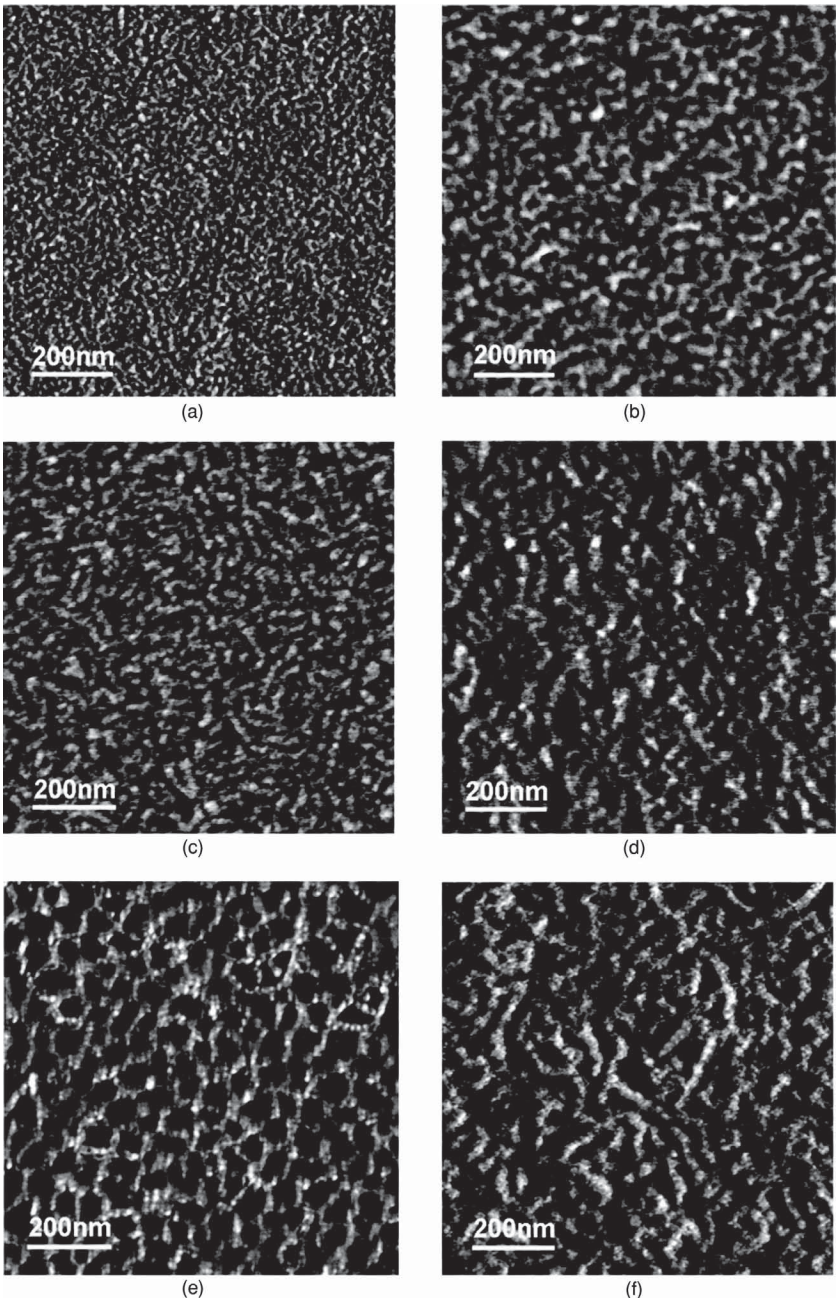

Figure 5. AFM phase morphologies of PS-*b*-P(St-*alt*-MA) block copolymer: a) BC_1; b) BC_2; c) BC_3; d) BC_4; e) BC_5; and f) BC6.

After that, the vessel was heated to 110 °C by oil bath lying in ventilating cabinet for 2 d. During this process, the MA experienced ring opening and became a carboxylate (carboxylic acid amine salt). Carboxylate is easily dissolved in water, and therefore the P(St-*alt*-MA) ionomers block were exposed to water vapor.

The AFM height images of the block ionomers shown in Figure S3 (Supporting Information) have a range of 9–80 nm. The height difference of the block ionomers samples increases with increasing P(St-*alt*-MA) ionomer block molecular weight. Figure 6 shows the AFM phase micrographs of the block ionomers after solvent annealing. From these phase micrographs, BI1, BI2, BI3, and BI6 form tightly packed droplet phases. The P(St-*alt*-MA) ionomers are a block and can easily be exposed to the water vapor atmosphere. This encases the PS microdomains in P(St-*alt*-MA) ionomers block. For BI4, well-ordered spherical P(St-*alt*-MA) ionomer block domains are embedded in a PS matrix and have a very short ionomer block. For BI5, the ionomer block is shorter than the PS block—a cylinder mixed with worm-like structures was observed. Therefore, the PS-*b*-P(St-*alt*-MA) block ionomers can easily form a corona structure around the PS core through microphase separation due to the matrix interfacial selectivity. Next, we discuss the advantages of microphase separation in the design of nucleation agents for PET crystallization.

3.4. Influence of PS-*b*-P(St-*alt*-MA) Block Ionomers on the Crystallization Behavior of PET

3.4.1. Isothermal Crystallization Behavior of PET and PET/BI Ionomers

We used DSC to investigate the crystallization behavior of PET influenced by our synthesized block ionomers. Studies of isothermal crystallization are often used to describe the nucleation type and growth rate.[51] In contrast to PET, PET with added BI can crystallize too fast at too low of a crystallization temperature to quench fast enough for the current generation of DSC equipment. This prevents samples from crystallizing before the target T_c is achieved. Therefore, we choose different isothermal crystallization temperature ranges for PET and PET with added BI. Although many methods and theories were used to study the isothermal crystallization, the Avrami analysis has been the most widely used approach to describe this information including analysis of nucleation mechanisms and comparison of polymer crystallization rates. Equation 3 is commonly called the Avrami equation.[52,53]

$$\ln\{-\ln[1-X(t)]\} = n\ln t + \ln K_t \quad (3)$$

Here, term $X(t)$ is the relative crystallinity at different crystallization times. The exponent n is the Avrami exponent. Term K_t is a growth rate constant involving both the nucleation and growth process. From a graphic representation of $\ln\{-\ln[1-X(t)]\}$ versus $\ln t$ according to Equation 3, the Avrami exponent n is valued as the slope of the straight line and the crystallization kinetic constant $\ln K_t$ as the intercept. In the induction period of crystallization, the crystal nucleus is unstable and easily melted by surrounding matrix. In the later stage of crystallization, the impingement of the two growing centers causes a cessation of their growth leading to large deviation from the Avrami theory. Therefore, to calculate the growth rate constant K_t and the half-time crystallization time $t_{1/2}$, the region $X(t)$ from 0.02 to 0.3 is selected and applied to the Avrami Equation 3 for PET crystallization in this paper.

Plots of $\ln\{-\ln[1-X(t)]\}$ versus $\ln t$ at different crystallization temperatures are shown in Figure S4 (Supporting Information), and the related parameters extracted from Figure S4 (Supporting Information) are summarized in Table 2. The results show that the Avrami exponents n for PET are over 3 at a low temperature and decrease with increasing isothermal temperature. The PET chains need a large supercooling to trigger 3D growth at higher temperatures. The n of PET with ionomers is about 2.5 at the crystallization temperature range we studied. This indicates that the nucleation type with nucleation agents is a heterogeneous nucleation controlled by large quantities of nuclei. In this case, the crystallization mode is not 3D but rather a mixture of 3D and 2D growth of nuclei due to impingement of adjacent spherical particles. The crystallization rate constant K_t and the half-time of crystallization $t_{1/2}$ are important indicators for characterizing the crystallization rate of polymers.

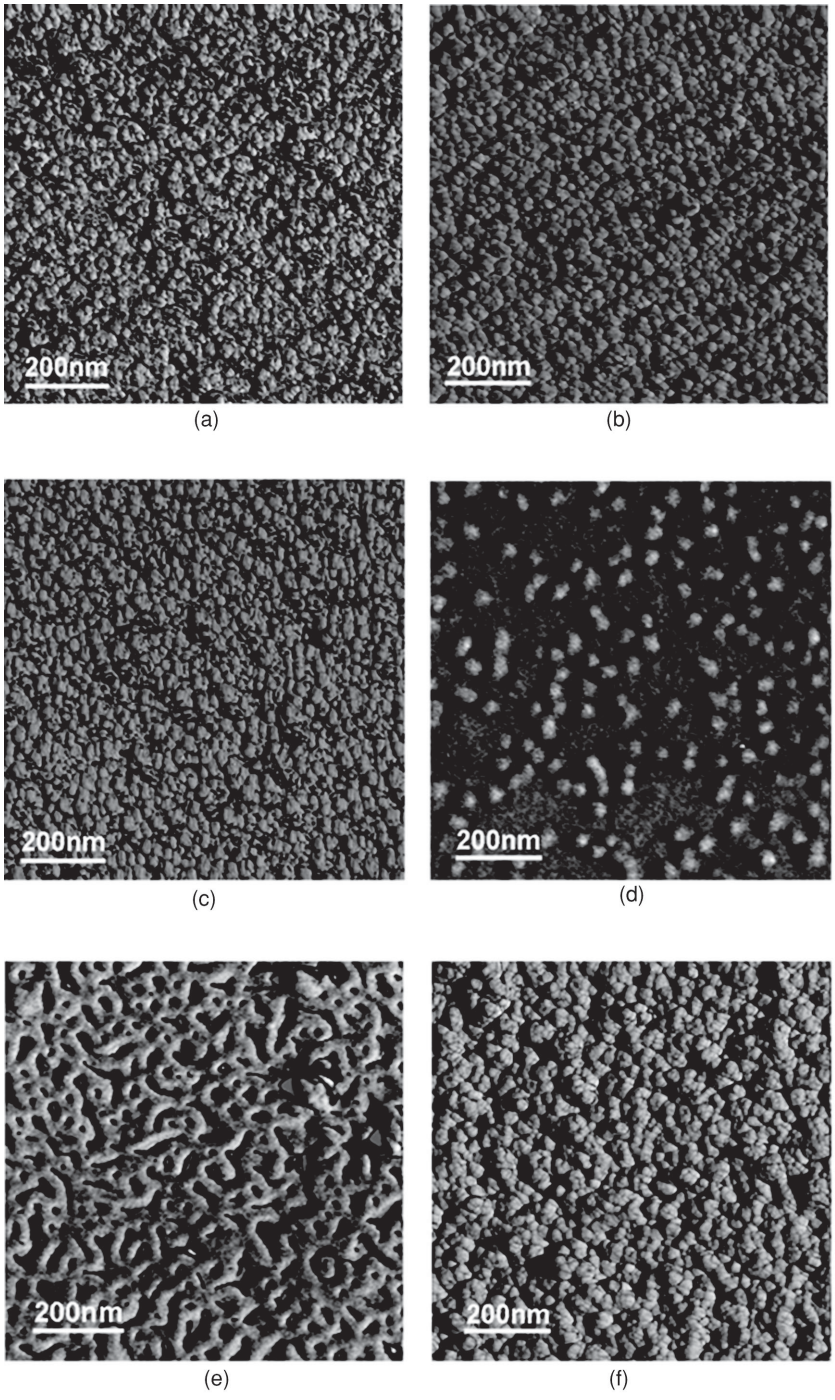

Figure 6. AFM phase morphologies of PS-*b*-P(St-*alt*-MA) block ionomers: a) BI1; b) BI2; c) BI3; d) BI4; e) BI5; and f) BI6.

Table 2 shows that the crystallization rate constant K_t of PET with ionomers increased, while the half-time of crystallization $t_{1/2}$ is reduced at high temperature. This indicates that the block ionomers indeed improve the crystallization rate of PET. We have studied that PET proceeds by both heterogeneous and homogeneous nucleation mechanisms during crystallization.[35] In the present work, BI produces microphase separation and serves as nucleation sites for PET crystallization. Therefore, the

crystallization of PET/BI samples proceeds mainly via heterogeneous nucleation and the number of heterogeneous nuclei is much larger than that in PET. Furthermore, the crystallization rate constant K_t and the crystallization half-time of PET/BI3 is higher than the other PET/BI samples and even higher than PET/Surlyn sample at the same isothermal crystallization temperature. The reason will be discussed later.

According to the classical crystallization theories, such as the Gibbs theory and Hoffman–Lauritzen theory, the driving force of polymer crystallization mainly comes from the internal energy in the system, which mainly relate with the crystallized entropy changes of the polymer chains from the disordered liquid (melt or solution) to the order solid phase (crystal), and from the rotation and rearrangement of the molecules at the surface of crystal or nucleus.[54] Therefore, the fold free energy is an important characterized parameter to measure the crystallization rate of polymers according the classic nucleation theory. The fold surface energy of samples was calculated via the Hoffman–Lauritzen theory[55] and the values are shown in Table 3, which clearly indicate that the nucleation agents indeed reduce the fold free energy of the polymers during the crystallization process but the values are different. For BI4, the lowest composition of P(St-*alt*-MA) block ionomers leads to the worst compatibility with PET matrix, thus having highest fold free energy than the others.

3.4.2. Non-isothermal Crystallization Behavior of PET and PET/BI Ionomers

Nonisothermal crystallization is more practical in polymer processing and more obvious on reflecting the effect of nucleation agents on the polymer crystallization.[54] In fact, nonisothermal crystallization usually carried out under constant cooling rate, the onset crystallization temperature $T_{on\ set}$, melting crystallization temperature T_{mc} and the halfway width of exothermal peak on cooling process can be obtained. Figure S5 (Supporting Information) shows nonisothermal melt crystallization curves of PET and PET with nucleation agents at 5 °C/min cooling rate. As expected, $T_{on\ set}$ and T_{mc} values shifted to high temperature, which means that the nucleation agents indeed improve the crystallization rate. The values of T_{mc} are shown in Table 3, the melting crystallization temperature of PET with nucleation agents was increased by 20 °C to 30 °C. Moreover, the values of the T_{mc} of the samples with block ionomers are even higher than the sample with Surlyn resin. This indicates that the effect of block ionomers on improving the crystallization rate of PET is superior to the Surlyn but the effects among the block ionomers are different. The sample with BI3 have the highest melting crystallization temperature, reflecting that the effect of BI3 on improving the crystallization behaviors is the best among these block ionomers, which is almost consistent with the results analyzing from the isothermal crystallization.

Table 2. Parameters of isothermal crystallization from the Avrami equation.

Sample	T_c [°C]	ln K_t	n	K_t	$t_{1/2}$ [s]
PET	210	−6.9	3.8	0.0011	332
	215	−9.0	3.6	1.21×10^{-4}	686
	220	−8.6	2.9	1.78×10^{-4}	1067
	224	−9.7	2.7	6.42×10^{-5}	1911
	226	−10.6	2.6	2.54×10^{-5}	2996
PET/Surlyn	226	−0.1	2.4	0.89	54
	228	−0.8	2.5	0.44	72
	230	−2.3	2.7	0.10	124
	232	−3.6	2.8	0.028	188
	234	−4.6	2.9	0.0097	258
PET/BI1	228	0.4	2.3	1.45	44
	230	−0.7	2.4	0.51	68
	232	−1.9	2.6	0.15	109
	234	−2.7	2.7	0.065	143
PET/BI2	228	−0.3	2.6	0.72	59
	230	−1.3	2.7	0.26	86
	232	−2.9	2.8	0.056	147
	234	−3.8	2.9	0.022	200
PET/BI3	228	0.1	2.4	1.10	49
	230	−0.2	2.6	0.82	56
	232	−1.4	2.8	0.24	87
	234	−1.9	2.9	0.14	103
PET/BI4	228	−1.1	2.3	0.32	84
	230	−1.7	2.4	0.18	105
	232	−2.2	2.5	0.11	125
	234	−3.8	2.8	0.022	210
PET/BI5	228	−0.7	2.4	0.49	69
	230	−1.9	2.5	0.16	108
	232	−2.1	2.7	0.12	115
	234	−3.1	2.8	0.044	159
PET/BI6	228	−0.8	2.6	0.47	70
	230	−1.6	2.7	0.20	95
	232	−2.8	2.8	0.062	143
	234	−4.1	2.9	0.016	216

Table 3. The fold free energy and the melting crystallization temperatures of samples.

Samples	σ_e [mJ m^{-2}]	T_{mc} [°C]
PET	110.6	189.2
PET/Suryln	47.1	222.9
PET/BI1	37.1	224.9
PET/BI2	42.3	224.4
PET/BI3	35.6	225.9
PET/BI4	47.9	224.5
PET/BI5	39.6	225.5
PET/BI6	38.4	223.4

According to the crystallization theory, effective nucleation agents for PET should have good compatibility with the PET matrix and blend upon melting with PET. Therefore, the compatibility of block ionomers with PET plays an important role in improving its crystallization behavior. To fundamentally understand the interfacial interactions between PET and PS-*b*-P(St-*alt*-MA) BCs, we carried out molecular dynamics (MD) to calculate the miscibility of experimentally prepared PET/SMA and PET/PS blends (Supporting Information).

We used the intermolecular radial distribution function (RDF) $g(r)$ of the carbon atoms between the polymer chains to analyze the compatibility of the polymer blends. The g(r) of the intermolecular atomic pairs indicates the interaction of polymers chains. If the g(r) of the polymer blend is lower than that of pure polymer, it indicates that the two polymers are poorly mixed. Meanwhile, if the g(r) of the polymer blend is higher than that of pure polymer, the two polymers have good compatibility.[56] Figure S7 (Supporting Information) shows that the g(r) of the intermolecular carbon atoms of PET/PET, PET/SMA, and PET/PS chains in blend systems. The g(r) curves of PET/PET and PET/SMA nearly coincide, and both of these two g(r) curves are higher than that of PET/PS (Figure S7, Supporting Information). This indicates that the PET/SMA blends have better compatibility than the PET/PS blends, which is consistent with reports by Yoon et al. based on experiment.[57]

Moreover, the effective nucleation agents should be solid phase and have good thermal stability at the crystallization temperature. Therefore, the degradation temperatures of block ionomers were measured by TGA (Figure S8, Supporting Information). It is clear that the degradation temperatures of these block ionomers are above 300 °C, which suggests that the ionomers remain solid without degradation during crystallization. The anhydride of P(St-*alt*-MA) has been salinized by sodium hydroxide and cannot be degraded, which leads to different residues among the PS-P(St-*alt*-MA) ionomers. As mentioned above, the ionomers can form nanostructures via microphase separation and the T_g of block ionomers is 241 °C, which remain solid state to act as nucleating sites for PET by providing more interfaces for crystal nucleus growth.

From Table 2 and Table 3, it is clear that the effect of block ionomers as nucleation agents for PET has a great relationship with the molecular weight ratios between two blocks and the molecular weights of the whole block ionomers. The P(St-*alt*-MA) ionomer block can interact with the PET chain and act as a nucleation agent for PET, but it needs excellent dispersion in the matrix. According to the Rouse model, the diffusion constant of the chain center of mass satisfies $D_G \propto M^{-1}$, i.e., it is inversely proportional to the molecular weight. Polymers with low molecular weight have better dispersion than those with high molecular weights when mixing in bulk.[58–60] For block ionomers, the P(St-*alt*-MA) ionomer block will be exposed to the PET matrix due to their mutual good compatibility while the PS block will be encased by the P(St-*alt*-MA) ionomer block through microphase separation. This will improve the dispersion of nucleation agents and increase the density of nucleation sites around the PS core.

However, for BI1 and BI2, polymers with low molecular weights have good dispersion, but it is difficult to form a microdomain through microphase separation in the PET matrix. Therefore, block ionomers need a PS block with a high molecular weight to form microdomains. For BI4, BI5, and BI6, an excessively long PS block will increase the P(St-*alt*-MA) ionomers molecular weight and correspondingly improve the molecular compatibility with PET matrix. This will decrease the molar concentration of the nucleation agent and the mobility of the whole block ionomers in PET matrix effectively reducing nucleation. Therefore, BI3 with suitable molecular weight and block ratio could form the microdomain through microphase separation and have great dispersion in PET matrix. Thus, BI3 is a better nucleation agent than the others.

4. Conclusion

According to the crystallization theory and our previous research, PS-*b*-P(St-*alt*-MA) block ionomers with the P(St-*alt*-MA) ionomer block having good compatibility with PET are designed for nucleating agents of PET. We suppose that the microphase-separated nanostructures in BCs provide heterogeneous nucleation sites for crystallization of PET. The purpose of salinization is to remain nucleating agents as a solid state during PET crystallization process by increasing the glass transition temperature of

P(St-*alt*-MA) block. This helps block ionomers induce PET chain arrangement and improve the crystallization rate. To investigate the effect of microphase morphologies of the nucleating agents on the crystalline behavior, the block ionomers with different molecular weights and ratios of PS block and P(St-*alt*-MA) block were synthesized by the two-step RAFT polymerization. The molecular weight and block ratios were controlled well by changing the feed ratio of monomers and reaction time. The PS-*b*-P(St-*alt*-MA) copolymers and their ionomers easily form nanostructures through microphase separation after thermal annealing. The crystallization behavior of PET with nucleation agents was studied isothermally based on the Avami and Hoffman–Lauritzen theories and non-isothermally by DSC. The results show that the block ionomers synthesized in our experiments act as nucleation agents to improve the crystallization behavior of PET. The nucleation efficiency strongly depends on the copolymer composition and the molecular weights. The effect of the block ionomer BI3 is even better than the commercial nucleation agent Surlyn resin and provides heterogeneous nucleation sites for crystallization of PET. These results offer new approaches for other new nucleation agents for other polymers.

Acknowledgements: The authors acknowledge financial support from the National Basic Research Program of China (Grant No. 2011CB605700). Funds from the NSF of China (Grant Nos. 20990231 and 91127033) are also acknowledged.

Received: August 26, 2014; Revised: September 26, 2014; Published online: November 10, 2014; DOI: 10.1002/macp.201400444

Keywords: block copolymers; ionomers; microphase separation; nucleation; poly(ethylene terephthalate) (PET)

[1] N. Hadjichristidis, S. Pispas, G. Floudas, *Block Copolymers: Synthetic Strategies, Physical Properties, and Applications*, John Wiley & Sons, Inc., Hoboken, NJ, USA **2003**, p. 386.
[2] B. Nandan, J. Y. Hsu, H. L. Chen*Polym. Rev.* **2006**, *46*, 143.
[3] L. Leibler, *Macromolecules* **1980**, *13*, 1602.
[4] R. A. Farrell, T. G. Fitzgerald, D. Borah, J. D. Holmes, M. A. Morris, *Int. J. Mol. Sci.* **2009**, *10*, 3671.
[5] F. S. Bates, G. H. Fredrickson, *Annu. Rev. Phys. Chem.* **1990**, *41*, 525.
[6] H. Hasegawa, H. Tanaka, K. Yamasaki, T. Hashimoto, *Macromolecules* **1987**, *20*, 1651.
[7] M. W. Matsen, M. Schick, *Phys. Rev. Lett.* **1994**, *72*, 2660.
[8] S. P. Liu, J. R. Ying, X. P. Zhou, X. L. Xie, Y. W. Mai, *Compos. Sci. Technol.* **2009**, *69*, 1873.
[9] A. R. Bhattacharyya, A. K. Ghosh, A. Misra, *Polymer* **2003**, *44*, 1725.
[10] K. J. Shelat, N. K. Dutta, N. R. Choudhury, *Langmuir* **2008**, *24*, 5464.
[11] B. Lessard, M. Maric, *Macromolecules* **2010**, *43*, 879.
[12] J. T. Han, P. Silcock, A. J. McQuillan, P. Bremer, *Colloid. Polym. Sci.* **2008**, *286*, 1605.
[13] D. Benoit, C. J. Hawker, E. E. Huang, Z. Lin, T. P. Russell, *Macromolecules* **2000**, *33*, 1505.
[14] M. Q. Zhu, L. H. Wei, M. Li, L. Jiang, F. S. Du, Z. C. Li, F. M. Li, *Chem. Commun.* **2001**, 365.
[15] A. P. Bapat, J. G. Ray, D. A. Savin, B. S. Sumerlin, *Macromolecules* **2013**, *46*, 2188.
[16] A. P. Bapat, J. G. Ray, D. A. Savin, E. A. Hoff, D. L. Patton, B. S. Sumerlin, *Polym. Chem.* **2012**, *3*, 3112.
[17] A. A. Vassiliou, K. Chrissafis, D. N. Bikiaris, *Thermochim. Acta* **2010**, *500*, 21.
[18] G. Antoniadis, K. M. Paraskevopoulos, A. A. Vassiliou, G. Z. Papageorgiou, D. Bikiaris, K. Chrissafis, *Thermochim. Acta* **2011**, *521*, 161.
[19] A. Durmus, N. Ercan, G. Soyubol, H. Deligoz, A. Kasgoz, *Polym. Compos.* **2010**, *31*, 1056.
[20] D. Garcia, *J. Polym. Sci., Part B: Polym. Phys.* **1984**, *22*, 2063.
[21] Y. N. Quan, H. H. Li, S. K. Yan, *Ind. Eng. Chem. Res.* **2013**, *52*, 4772.
[22] L. H. Sperling, *US* 5356972, **1994**.
[23] Y. C. Ke, T. B. Wu, Y. F. Xia, *Polymer* **2007**, *48*, 3324.
[24] Y. Yu, H. S. Bu, *Macromol. Chem. Phys.* **2001**, *202*, 421.
[25] H. Cartier, *US* 7015267, **2002**.
[26] X. Pang, L. Zhao, M. Akinc, J. K. Kim, Z. Lin, *Macromolecules* **2011**, *44*, 3746.
[27] X. C. Pang, C. W. Feng, H. Xu, W. Han, X. K. Xin, H. P. Xia, F. Qiu, Z. Q. Lin, *Polym. Chem.* **2014**, *5*, 2747.
[28] N. V. Salim, T. Hanley, Q. P. Guo, *Macromolecules* **2010**, *43*, 7695.
[29] A. Boschetti-de-Fierro, A. T. Lorenzo, A. J. Muller, H. Schmalz, V. Abetz, *Macromol. Chem. Phys.* **2008**, *209*, 476.
[30] C. Park, C. De Rosa, B. Lotz, L. J. Fetters, E. L. Thomas, *Macromol. Chem. Phys.* **2003**, *204*, 1514.
[31] N. Hosoda, E. H. Lee, T. Tsujimoto, H. Uyama, *Ind. Eng. Chem. Res.* **2013**, *52*, 1548.
[32] A. T. Lorenzo, M. L. Arnal, A. J. Muller, A. Boschetti-de-Fierro, V. Abetz, *Macromolecules* **2007**, *40*, 5023.
[33] Y. T. Chen, C. T. Lo, *Soft Matter* **2013**, *9*, 1756.
[34] X. C. Pang, L. Zhao, W. Han, X. K. Xin, Z. Q. Lin, *Nat. Nanotechnol.* **2013**, *8*, 426.
[35] S. L. Xing, P. Tang, Y. L. Yang, *J. Appl. Polym. Sci.* **2015**, *132*, 41240.
[36] R. T. Yu, S. X. Zheng, *Macromolecules* **2012**, *45*, 9155.
[37] L. T. Phuong, M. Graeme, R. Ezio, T. S. Hoa, *WO 1998001478 A1*, **1998**.
[38] M. C. Davies, J. V. Dawkins, D. J. Hourston, *Polymer* **2005**, *46*, 1739.
[39] S. D. Baruah, N. C. Laskar, *J. Appl. Polym. Sci.* **1996**, *60*, 649.
[40] G. Karakus, A. F. Yenidunya, H. B. Zengin, Z. A. Polat, *J. Appl. Polym. Sci.* **2011**, *122*, 2821.
[41] G. R. Saad, R. E. Morsi, S. Z. Mohammady, M. Z. Elsabee, *J. Polym. Res.* **2008**, *15*, 115.
[42] R. Ma, R. M. Ma, L. L. Feng, L. R. Fan, Y. Liu, B. Xing, Y. B. Hou, F. Bao, *Colloid Surf. A* **2009**, *346*, 184.
[43] M. Ignatova, O. Stoilova, N. Manolova, D. G. Mita, N. Diano, C. Nicoiucci, I. Rashkov, *Eur. Polym. J.* **2009**, *45*, 2494.
[44] G. B. Butler, C. H. Do, M. C. Zerner, *J. Macromol. Sci. Chem.* **1989**, *A26*, 1115.
[45] Y. J. Nie, H. H. Gao, M. H. Yu, Z. M. Hu, G. Reiter, W. B. Hu, *Polymer* **2013**, *54*, 3402.
[46] R. D. Spaans, M. Muhammad, M. C. Williams, *J. Polym. Sci., Part B: Polym. Phys.* **1999**, *37*, 267.
[47] A. D. Pasquino, M. Pilswort, *J. Polym. Sci., Part B: Polym. Lett.* **1964**, *2*, 253.
[48] Y. Qu, F. Huo, Q. Li, X. He, S. Li, W. Zhang, *Polym. Chem.* **2014**, *5*, 5569.
[49] P. P. Chen, X. Huang, Q. H. Zhang, K. Xi, X. D. Jia, *Polymer* **2013**, *54*, 1091.
[50] C. M. Bates, T. Seshimo, M. J. Maher, W. J. Durand, J. D. Cushen, L. M. Dean, G. Blachut, C. J. Ellison, C. G. Willson, *Science* **2012**, *338*, 775.

[51] P. Varma, E. A. Lofgren, S. A. Jabarin, *Polym. Eng. Sci.* **1998**, *38*, 237.
[52] M. J. Avrami, *Chem. Phys.* **1941**, *9*, 177.
[53] M. J. Avrami, *Chem. Phys.* **1939**, *7*, 1103.
[54] Y. Long, R. A. Shanks, Z. H. Stachurski, *Prog. Polym. Sci.* **1995**, *20*, 651.
[55] L. Mandelkern, *Crystallization of Polymers, Vol. 2: Kinetics and Mechanisms*, Cambridge University Press, Cambridge, UK **2004**, p. 5.
[56] E. D. Akten, W. L. Mattice, *Macromolecules* **2001**, *34*, 3389.
[57] K. H. Yoon, H. W. Lee, O. O. Park, *Polymer* **2000**, *41*, 4445.
[58] R. Gelles, C. W. Frank, *Macromolecules* **1983**, *16*, 1448.
[59] Y. Feng, C. C. Han, M. Takenaka, T. Hashimoto, *Polymer* **1992**, *33*, 2729.
[60] M. Doi, S. F. Edwards, *The Theory of Polymer Dynamics*, Oxford University Press, New York **1986**, p. 46.